RESEARCH ARTICLE

3D–3D Rigid Registration of Echocardiographic Images With Significant Overlap Using Particle Filter

THANUJA URUTHTHIRAKODEESWARAN[1], (Member, IEEE), **MICHELLE NOGA**[1],
LAWRENCE H. LE[1], **PIERRE BOULANGER**[2], (Member, IEEE), **HARALD BECHER**[3],
AND KUMARADEVAN PUNITHAKUMAR[1,2], (Senior Member, IEEE)

[1]Department of Radiology and Diagnostic Imaging, University of Alberta, Edmonton, AB T6G 2B7, Canada
[2]Department of Computing Science, University of Alberta, Edmonton, AB T6G 2E8, Canada
[3]Division of Cardiology, Mazankowski Alberta Heart Institute, Edmonton, AB T6G 2B7, Canada

Corresponding author: Thanuja Uruththirakodeeswaran (uruththi@ualberta.ca)

ABSTRACT The precise alignment of 3D echocardiographic images taken from different views has been shown to enhance image quality and increase the field of view. This study proposes a novel sequential Monte Carlo (SMC) algorithm for the 3D-3D rigid registration of echocardiographic images with significant overlap that is robust to the noise present in ultrasound images. The algorithm estimates the translational and rotational components of the rigid transform through an iterative process and requires an initial approximation of the rotation and translation limits that depend on the dimension of the image and the initial overlap between images. The registration is performed in two ways: the same transform approach applies the transform computed for the end diastolic frame to all frames of the cardiac cycle, whereas the unique transform approach registers each frame independently. The proposed SMC and exhaustive search algorithms were evaluated for 3D transthoracic echocardiographic volumes recorded from 3 patients and 3 volunteers who participated in two different research studies conducted at the Mazankowski Alberta Heart Institute. The evaluations demonstrate that the same transform approach yielded a Dice score value of 0.716 ± 0.041 for the left ventricle and required less computational time than the unique transform approach or exhaustive search. It was found that the SMC algorithm performs better than the exhaustive search at the 0.05 significance level using the paired t test. The accuracy was improved further using the Simple Elastix non-rigid registration algorithm to fix misalignments due to movement and breathing, with an overall Dice score value of 0.787 ± 0.038.

INDEX TERMS Sequential Monte Carlo, particle filter, 3D-3D rigid registration, echocardiographic images.

I. INTRODUCTION

According to the World Health Organization, heart disease is a major challenge for healthcare systems [1], and it is the second leading cause of death in Canada [2]. An accurate and timely diagnosis of cardiac disease is essential for a healthy life. Cardiac images are analyzed by healthcare

The associate editor coordinating the review of this manuscript and approving it for publication was Orazio Gambino.

practitioners for clinical diagnosis, prognosis, planning and guiding treatment, monitoring disease progression, and other follow-up processes, as well as scientific purposes. Ultrasound (US) is widely used to obtain cardiac images compared to magnetic resonance imaging (MRI), computed tomography (CT), cone beam CT (CBCT) and positron emission tomography (PET) to analyze the structure and function of the heart due to its high temporal resolution, portability, accessibility, and affordability. In addition, the

US uses non-ionizing examinations compared to CT, CBCT, and PET modalities. Although it provides real-time images, analyzing raw ultrasound images is not easy because of the low imaging quality due to the noise level and presence of artifacts, the high dependence on operator/diagnostician experience, and the high variability across different US manufacturers' systems [3], [4], [5].

Despite its widespread use, ultrasound imaging of the heart suffers from a limited field of view, and only a portion of the heart is often imaged in a single scan due to this limitation. Although three dimensional (3D) ultrasound scans offer a better field of view than two-dimensional (2D) ultrasound scans that image only a slice of the heart, it is not possible to scan the entire heart in a single 3D scan most of the time. The field of view limitation could be overcome by acquiring images from different positions that require an approach to precisely align images for clinical tasks. In addition, image segmentation and fusion may require image registration as a preprocessing step. The performance of a registration algorithm is critical for using aligned 3D datasets for diagnostic purposes.

Image registration is the process of aligning two or more images into the same geometric coordinate system to determine the feature or intensity correspondence between images. It is required to precisely align the images for clinical tasks that use computer systems to visualize overlapped images [6], as these images are taken at different times from different views using the same or different modalities. Techniques used to register images differ depending on input image modalities, dimensions, region of interest, nature of the information, required transform type, optimization methods, and interaction level [7], [8].

Rigid registration uses translation and rotation to transform one image into another, and it can be used as a global preregistration of images for non-rigid registration. The rigid registration can be used for the alignment of intrapatient images and the registration of multimodal images when considering its application to medical images [8]. A 2D echocardiographic image has limited details compared to a 3D image which is considered a sequence of 2D images with great depth of view from any spatial point. 3D transthoracic echocardiographic (3DE) imaging with its advanced probes and image acquisition techniques helps to overcome the issues in analyzing 2D images with geometric assumptions [9]. There are various classical and modern image registration techniques that are used to align images, which support parallel processing with Graphical Processing Unit (GPU) hardware, and they are more computationally efficient compared to non-parallel or CPU based implementations [10].

Classical image registration algorithms use energy functions to calculate the transform model, and single pairwise image registration can be performed using these algorithms in an iterative manner with limited computing resources [11]. The particle filter (PF) approach is a technique for implementing a recursive Bayesian filter by Monte Carlo (MC) sampling, which represents posterior density by a set of random particles with associated weights. The advantage of using the Bayesian filtering framework for image registration is its ability to handle outliers and local minima convergence while being robust to noise [12]. The PF is a nonlinear and non-Gaussian filter that processes data sequentially. The basic steps of the PF approach are to generate a bunch of random particles, predict the next state of particles, update particle weights, resample particles, and compute estimates [13]. The last four steps will be followed repeatedly until the required accuracy is achieved while overcoming the challenges of PF which are particle degeneracy, sample impoverishment, particle divergence, selecting importance density, and real time execution [14], [15].

There has been limited research conducted using MC based approaches for both 2D and 3D multi-modality medical images [12], [16], [17], [18], [19], [20] and parallel architecture support for these algorithms is being explored now. The number of experimental studies [13], [14], [15], [21] showing the use of MC algorithms for image registration suggests that this new area is worth exploring. Wong [16] proposed a method to use an adaptive MC method for registering 2D multimodality images (T1-T2 MRI and T1 MRI-PET) using non-parallel hardware. In another study [17], the affine transform was performed using the particle filter algorithm to register 2D and 3D non-US multimodality images such as MRI, CT, proton density (PD), and PET in a non-parallel architecture. The particle flow filter [12] was used for rigid registration of 2D MRI images and 2D-2D and 2D-3D non-medical images using non-parallel hardware. Other studies [18] and [19] proposed non-rigid registration algorithms for 2D CT and MRI images using the particle filter and particle swarm optimization approaches, respectively. The particle swarm optimization approach uses particles with velocities, which is fundamentally different from the particle filter or sequential MC approach proposed for the image registration problem in this study. A stochastic gradient Markov Chain MC approach [20] was used to align 3D brain MRI data using a non-rigid registration algorithm and the performance was evaluated in both parallel and non-parallel architectures against variation inference and the voxelmorph [22] approach. A recent study [23] proposed landmark based rigid registration approach for 3D-3D echocardiographic images as monomodality using reinforcement learning. To the best of the authors' knowledge, there has been no method proposed to register 3D-3D echocardiographic images as mono/multimodality using MC methods. This study proposes a sequential MC approach to register the temporal sequence of echocardiographic volumes with significant overlap using intensity based rigid registration.

II. METHODOLOGY
A. PROBLEM FORMULATION
Accurate alignment of 3DE images, captured from various views and at different time points, is crucial for whole

heart clinical analysis. The intensity based rigid registration algorithm proposed in this study for 3DE images of different views is significant, as there are no algorithms available now for either the CPU or GPU architecture. With the combination of a novel rigid registration algorithm and a non-rigid algorithm, better performance can be achieved with less computational time for 3DE images.

3DE images are acquired in the parasternal long axis, parasternal short axis, and apical planes in general to perform volume analysis of heart chambers, calculate ejection fraction (EF), and assess the functions of the heart valves [9], [24], [25]. The apical view of 3DE provides better visualization of four chambers compared to other views [9], [26] and this study focuses on full volume images acquired on the apical plane. The apical standard and non-standard images are used to calculate the volume of the left ventricle (LV) and EF, and analyze effective orifice area [27].

The sequential MC approach is a new concept to explore with 3D image registration as it is widely used for state estimation in 2D. The PF algorithm proposed in this research for 3DE image registration using non-parallel architecture was designed and developed from scratch and is an innovative approach.

B. REGISTRATION

The rigid registration is performed on 3DE images with significant overlap using the PF algorithm. The apical standard and non-standard images of the same patient are considered images with significant overlap to perform registration with translation and rotation. The voxel intensity is considered alone to perform the task without using landmarks or features. The objective of the registration algorithm is to find the best transform ($\hat{\phi}$) that minimizes the dissimilarity value between source (S) and target (T) images when applying transform ϕ.

$$\hat{\phi} = \arg \min_{\phi} E_D\left(I_T, I_S(\phi)\right) \tag{1}$$

The PF estimates the rigid transform required to align the source image to the target image using weighted particles over iterations using the transform as state and the dissimilarity value between the source and the target image as measurement. A bunch of particles (N) are generated using a uniform distribution with rotation (r_x, r_y, r_z) and translation (t_x, t_y, t_z) values in the x, y, and z axes within a given interval [min, max]. The state represented by each particle x^i is defined as ($r_x, r_y, r_z, t_x, t_y, t_z$) denoting the six degrees of freedom for 3D-3D rigid registration. Each parameter (p) of the transform for a particle can be defined as in (2) for initialization with minimum and maximum thresholds a and b. The state at time k is defined as (3) where I_6 is the 6×6 identity matrix and v_{k-1} is an independent and identically distributed (i.i.d) process noise sequence composed of six parameters of a 3D rigid transform approximated by Gaussian distribution. The measurement (z) at time k is defined as (4) where H_k is the function that calculates the dissimilarity value between the source image at time k and the target image, and

v_k is i.i.d measurement noise.

$$p \sim U(a, b) \tag{2}$$

$$x_k = I_6 x_{k-1} + v_{k-1} \tag{3}$$

$$z_k = H_k x_k + n_k \tag{4}$$

The prediction, update, resampling, and estimation steps of PF are performed iteratively once the state space is initialized with a uniform distribution and a minimum dissimilarity value of -1 as the initial measurement as shown in Figure 1. The prediction step finds the state at time k with measurements available up to time $k - 1$ using the prior probability density function (pdf) (5) where $\delta(.)$ is the Dirac delta measure and $w^i_{k:k-1}$ (6) is the conditional probability of the state given measurements up to time $k - 1$. The weight of particle i at time k is denoted as w^i_k and the weights are normalized such that $\sum_{i=1}^{N} w^i_k = 1$. The weights of the particles are updated using the new measurement z_k and the posterior state is defined (7) during the update step where $w^i_{k:k}$ value is defined as (8).

$$p\left(x_k \mid z_{1:k-1}\right) \approx \sum_{i=1}^{N} w^i_{k:k-1} \delta\left(x_k - x^i_{0:k}\right) \tag{5}$$

$$w^i_{k|k-1} \triangleq \sum_{j=1}^{N} w^j_{k-1|k-1} p\left(x^i_k \mid x^j_{k-1}\right) \tag{6}$$

$$p\left(x_k \mid z_{1:k}\right) \approx \sum_{i=1}^{N} w^i_{k:k} \delta\left(x_k - x^i_{0:k}\right) \tag{7}$$

$$w^i_{k|k} \triangleq \frac{w^i_{k|k-1} p\left(z_k \mid x^i_k\right)}{\sum_{j=1}^{N} w^j_{k|k-1} p\left(z_k \mid x^j_k\right)} \tag{8}$$

$$p\left(x_k \mid z_{1:k}\right) \approx \sum_{i=1}^{N} w^i_k \delta\left(x_k - x^i_k\right) \tag{9}$$

$$T = \sum_{i*=1}^{N} x^{i*}_k w^{i*}_k \tag{10}$$

To avoid particle degeneracy, the particles are resampled as the next step using systematic resampling (9), where particles with lower weights are replaced by particles with higher weights if the number of effective particles falls below a threshold value, and results in a new particle set $\{x^{i*}_k\}_{i=1}^{N}$ with each particle having the same weight as $1/N$. In the last step of the iteration, the components of the transform are estimated as the mean value of states represented by weighted particles (10). The accuracy of the registration algorithm is evaluated using a similarity metric and an overlap score because the similarity metric alone is not sufficient to estimate the accuracy of the algorithm [28].

C. DATASET

The 3D transthoracic echocardiography dataset was obtained as part of two research studies conducted at the Mazankowski Alberta Heart Institute and both studies were approved by
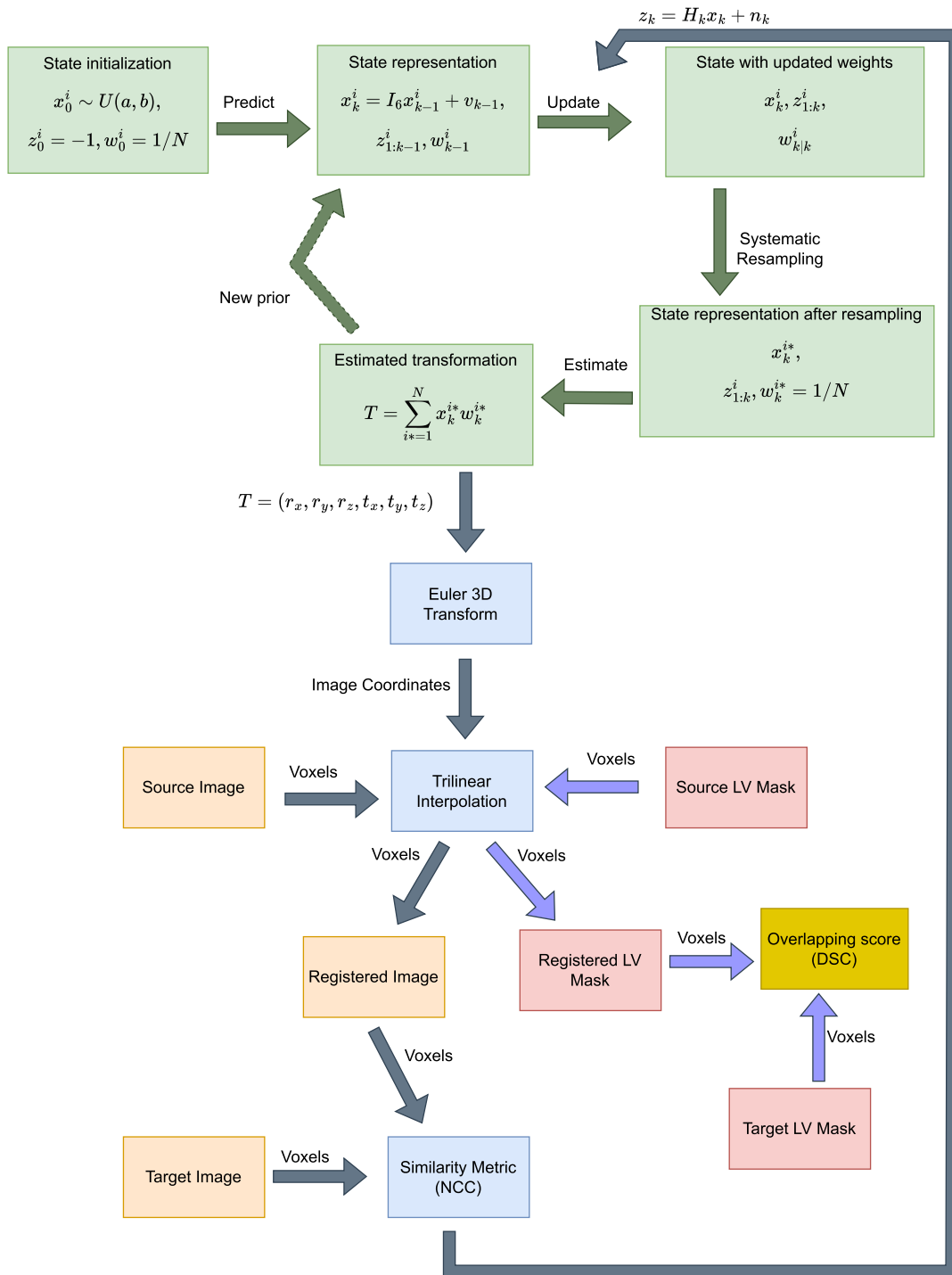
FIGURE 1. The 3D-3D rigid registration using PF algorithm where the state of the system is represented by N particles (x^i) and its associated weights (w^i) are highlighted along with the measurement values (z^i) after prediction, update, resampling, and estimation steps. The estimated transform by the PF algorithm is used to register the source image with the target image. The same transform is used to calculate the Dice score value between the LV masks of the source and target images. The similarity metric value between the source and the target is used as the measurement value when updating the weights in the next iteration.

the Health Research Ethics Board of the University of Alberta. As part of the first research study, images were obtained manually by a sonographer using a Philips X5-1 probe and a Philips EPIQ 7C scanner (Philips Healthcare, Eindhoven, The Netherlands). There were 7 image pairs from 3 patients (gender ratio: 2 female and 1 male; age range: 19

to 32) considered to evaluate the registration algorithm using 210 frames with an average frame rate of 25.13. To increase the number of source and target image pairs, the images were swapped between them to get 14 image pairs over 420 frames. The second research study used a robotic arm to obtain images in a controlled manner with less strain on the sonographer using the same ultrasound probe and machine [29]. There were 30 image pairs from 3 volunteers (gender ratio: 3 male, age range: above 18) considered to evaluate the algorithm using 503 frames with an average rate of 19.75. The details of image acquisition and volume metadata are listed in Table 1. The second image of the third patient was resized to $272 \times 176 \times 206$ voxel size with resampling. There were 310, 52, and 58 frames considered from each patient while 189, 188, and 126 frames were for each volunteer. The binary masks of the left ventricle (LV) area were annotated by a sonographer and used after the registration to validate the performance of the algorithm by applying the transform to the mask of the source image to be considered as the registered mask to calculate the overlapping score after each iteration as shown in Figure 1.

D. IMPLEMENTATION DETAILS

The PF algorithm was implemented using the Python (3.9.6) language with the ITK (5.2.1) v4 framework. Normalized cross-correlation (NCC) (11) was used to assess the similarity between the source and target images. The Euler 3D transform was used to find the rigid transform (1) that calculates new image coordinates after applying the rigid transform $(r_x, r_y, r_z, t_x, t_y, t_z)$ as defined in (12), as shown at the bottom of the next page. The source image was aligned with the target image using trilinear interpolation to find voxel values at non-grid positions, reducing dissimilarity between the images recursively.

$$NCC_{v4}(T, S) = \frac{\left(\sum_{i=1}^{N} \left(T_i - \bar{T}\right) \left(S_i - \bar{S}\right)\right)^2}{\sum_{i=1}^{N} \left(T_i - \bar{T}\right)^2 \sum_{i=1}^{N} \left(S_i - \bar{S}\right)^2} \quad (11)$$

There were two approaches followed to perform the registration: the unique transform approach and the same transform approach as shown in Figure 2. When considering the unique transform approach, each frame of the source and target images is registered independently over a cardiac cycle. The same transform approach finds the rigid transform to register end-diastolic (ED) frames and applies the same transform to all the other frames in the cardiac cycle.

The number of particles (N) used for the algorithm was defined as 1000 to represent the 3D state space, while the translation and rotation limits were defined as $(-5, 5)$ mm and $(-60, 60)$ degrees considering the image size and initial overlap between the source and target images. The state process noise in (3) was approximated by a Gaussian distribution with a mean of 0 and rotation and translation standard deviations of 1 degree and 2 mm, respectively. The weights of particles were approximated by a Gaussian distribution, with the measurement as the mean and the

weight standard deviation of 0.1. The threshold for effective particles is set to $N/2$ for the resampling step. Since the non-parallel version of the PF algorithm is used in this study for rigid registration, the number of iterations is limited to 10 while reporting the results here.

The nonrigid Simple Elastix (SE) [30] registration was implemented using Simple ITK 2.2.1 for the same Python version to improve the registration accuracy after performing rigid registration. The advanced normalized correlation and transformed bending energy penalty were used as metrics to perform multi-metric, multi-resolution registration using a recursive image pyramid. The registration was performed for 100 iterations for each of the 5 levels of resolution.

E. BASELINE AND EVALUATION METRICS

The accuracy of registration is evaluated using the NCC as the similarity metric and the Dice score (DSC) as the overlapping score. The similarity between images is measured on a scale from 0 to 1, where 1 indicates a high correlation between voxel intensities and proper alignment. The DSC between the 3D binary masks of the source and target images S and T is defined as (13) where a value of 0 indicates that there is no overlap between the corresponding images and a value of 1 indicates that the images are perfectly aligned.

$$Dice\ score(S, T) = \frac{2 * |S \cap T|}{|S| + |T|} \quad (13)$$

The exhaustive search (ES) method is used as a baseline method to compare the accuracy of the PF algorithm and was implemented using the ITK (5.2.1) v4 framework's exhaustive optimizer [31] for the same Python version. The step size of the ES was defined as 2 in all three dimensions while keeping rotation scaling at 0.05 and translation scaling at 1.0 with an optimizer step length of 1. The registration was initialized using the centroid transform initializer. These values were defined to obtain better performance over reasonable computation time compared to the PF algorithm, and the ES method used 15625 iterations while PF used 10 iterations to register images. Both the unique and the same transform approaches were used to evaluate the accuracy of the PF and ES algorithms.

III. RESULTS

The average similarity metric (NCC) and the overlapping score (DSC) changes before and after the registration are listed in Table 2 for the unique and the same transform approaches of both the PF and ES algorithms for 420 frames of the patient dataset. Figure 3 shows the DSC values for both methods that are summarized in Table 3 for the minimum, 25%, 50%, 75%, and maximum DSC values. The student paired t test was performed to evaluate the significance of the PF and ES algorithms, and it was found that PF results are significant compared to ES, with a p value of 0.00023 at the 0.05 significance level. This shows that the PF method outperforms the ES in terms of registration accuracy evaluated using DSC. Furthermore, the

TABLE 1. The metadata of image sequences of 3 patients (P1, P2, P3) and 3 volunteers (V1, V2, V3).

Participant ID	No. of 4D sequence	Acquisition type	Frame rate	Volume size (voxel)	Volume resolution (mm)
P1	5	HMQ	22	$272 \times 176 \times 208$	$0.73 \times 1.13 \times 0.73$
P2	2	4Q	35	$272 \times 176 \times 208$	$0.77 \times 1.21 \times 0.78$
P3	1	4Q	34	$272 \times 176 \times 208$	$0.77 \times 1.21 \times 0.78$
P3	1	4Q	32	$288 \times 176 \times 208$	$0.82 \times 1.28 \times 0.82$
V1	6	HMQ	22	$224 \times 176 \times 208$	$0.87 \times 1.08 \times 0.73$
V2	7	HMQ	20	$224 \times 176 \times 208$	$0.98 \times 1.21 \times 0.82$
V3	6	HMQ	16	$224 \times 208 \times 208$	$1.09 \times 1.30 \times 0.92$
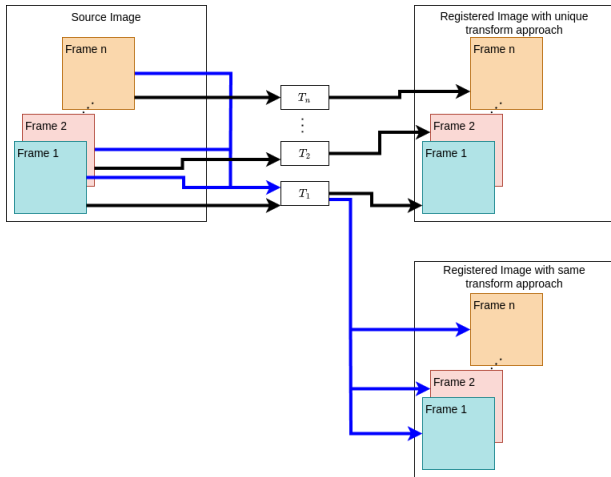
FIGURE 2. The unique vs. same transform approach followed to register *n* frames of a temporal sequence using the PF algorithm. T_1, T_2 up to T_n denote the transforms estimated recursively by the algorithm.

TABLE 2. The similarity metric (NCC) and overlapping score (DSC) changes before and after rigid registration for patient dataset. The best results are highlighted for rigid registration.

Metric	Method	Value
NCC	Initial	0.647 ± 0.020
	PF_u	0.693 ± 0.029
	ES_u	0.601 ± 0.011
	PF_s	**0.698 ± 0.012**
	ES_s	0.589 ± 0.011
	PF_s + Simple Elastix	0.720 ± 0.009
DSC	Initial	0.677 ± 0.037
	PF_u	**0.744 ± 0.043**
	ES_u	0.700 ± 0.048
	PF_s	0.743 ± 0.041
	ES_s	0.669 ± 0.051
	PF_s + Simple Elastix	0.791 ± 0.042

same transform approach performs better than the unique transform approach when registering a sequence of 3D frames (temporal frames) for a cardiac cycle using rigid registration, considering the time taken to register images by the unique transform approach was approximately *n* times that of the same transform approach, where *n* is the number of frames in a cardiac cycle. The computational time of both the PF and ES algorithms is presented at the end of this section. The deformation of frames within the cardiac cycle of the source and the target images due to patient movement and respiration cannot be aligned using rigid registration and a non-rigid registration is required for that purpose. We used Simple Elastix registration after rigid registration to improve the accuracy for PF with the same transform approach results and obtained improved results as listed in Table 2 and Figure 3.

The average NCC changes for the unique and the same transform approaches are shown in Figure 4. The NCC value increases over iterations even though there was a drop at the first iteration because the algorithm uses the uniform distribution of particles with equal weights as the state initialization. Further, the correlation between the similarity


FIGURE 3. The 3D-3D rigid registration results using the PF and ES algorithms for the patient dataset. The figure shows the DSC before registration (initial) and after registration using unique (u) vs. same (s) transform approaches for the PF and ES algorithms. The DSC after rigid and non-rigid registration for PF with the same transform approach and Simple Elastix (SE) registration is shown as the last plot.

metric (NCC) and overlapping score (DSC) was analyzed. Figure 5 shows DSC changes over iterations, and it is found that the average DSC value drops for the first iteration similar
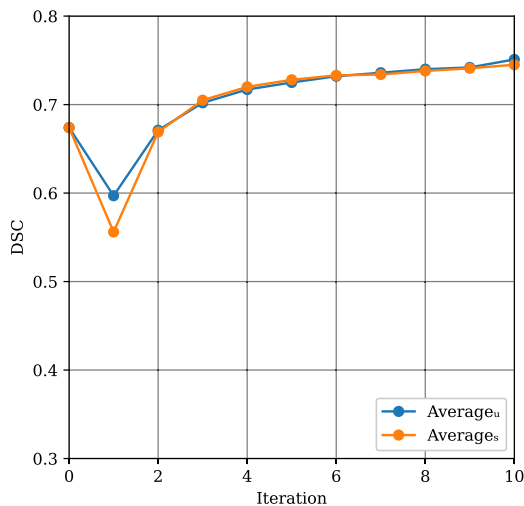
$$\begin{bmatrix} x' \\ y' \\ z' \end{bmatrix} = \begin{bmatrix} 1 & 0 & 0 \\ 0 & \cos r_x & -\sin r_x \\ 0 & \sin r_x & \cos r_x \end{bmatrix} \begin{bmatrix} \cos r_y & 0 & \sin r_y \\ 0 & 1 & 0 \\ -\sin r_y & 0 & \cos r_y \end{bmatrix} \begin{bmatrix} \cos r_z & -\sin r_z & 0 \\ \sin r_z & \cos r_z & 0 \\ 0 & 0 & 1 \end{bmatrix} \begin{bmatrix} x \\ y \\ z \end{bmatrix} + \begin{bmatrix} t_x \\ t_y \\ t_z \end{bmatrix} \tag{12}$$

TABLE 3. The rigid registration results for image pairs of patient data using mean DSC for minimum, maximum, and percentile values. The best results are highlighted for each category.

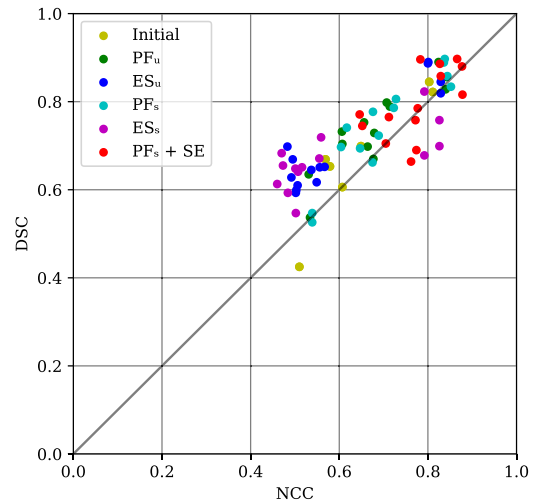| Method	Min	Q1(25%)	Q2 (50%)	Q3(75%)	Max
Initial DSC	0.425	0.606	0.669	0.822	0.845
PF_u	0.537	0.698	0.743	0.828	0.890
ES_u	0.593	0.617	0.652	0.819	0.890
PF_s	0.526	0.694	0.745	0.834	**0.897**
ES_s	0.547	0.641	0.663	0.699	0.823
PF_s + Simple Elastix	**0.664**	**0.745**	**0.778**	**0.880**	**0.897**
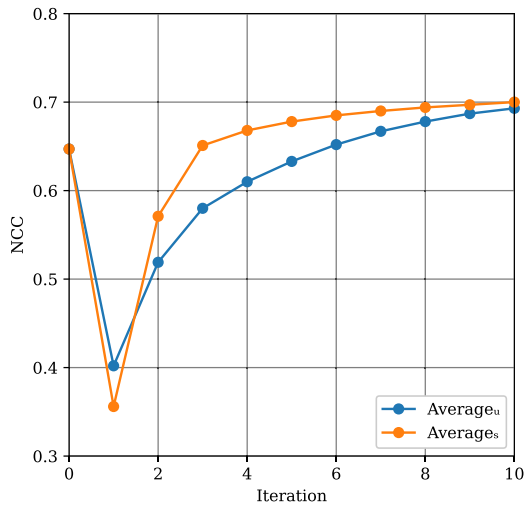
FIGURE 4. The average similarity metric value over iterations for PF using unique (u) vs. same (s) transform approaches. Iteration 0 shows the NCC value before registration.

FIGURE 6. The correlation between overlapping score (DSC) and similarity metric (NCC) of PF, ES, and PF + SE methods for patient data.

TABLE 4. The similarity metric (NCC) and overlapping score (DSC) changes before and after rigid registration for patient and volunteer dataset. The best results are highlighted for rigid registration.

Metric	Method	Value
NCC	Initial	0.657 ± 0.015
	PF_s	**0.681 ± 0.011**
	ES_s	0.612 ± 0.010
	PF_s + Simple Elastix	0.741 ± 0.010
DSC	Initial	0.641 ± 0.041
	PF_s	**0.716 ± 0.041**
	ES_s	0.660 ± 0.048
	PF_s + Simple Elastix	0.787 ± 0.038

FIGURE 5. The overlapping score (DSC) value over iterations for PF using unique (u) vs. same (s) transform approaches. Iteration 0 shows the DSC value before registration.

to Figure 4 for the same reason. The NCC and DSC value changes over iteration for the ES method are not considered because of the high number of iterations. The correlation between DSC and NCC for approaches listed in Table 2 is

shown in Figure 6, and it is found that the correlation value between DSC and NCC is 0.84.

The PF algorithm with the same transform approach was evaluated further using the volunteer dataset against the baseline method and the results for 3 patients and 3 volunteers are listed in Table 4. Figure 7 shows the DSC values for both methods that are summarized in Table 5 for the minimum, 25%, 50%, 75%, and maximum DSC values. The images before and after registration using PF, ES and PF + SE methods for the pairs listed in Table 5 are shown in

TABLE 5. The rigid and non-rigid registration results for image pairs of patient and volunteer data using mean DSC for minimum, maximum, and percentile values. The best results are highlighted for each category.

Method	Min	Q1(25%)	Q2 (50%)	Q3(75%)	Max
Initial DSC	0.425	0.535	0.631	0.699	0.845
PF_s	0.526	0.661	0.696	0.777	**0.897**
ES_s	0.529	0.587	0.668	0.741	0.823
PF_s + Simple Elastix	**0.657**	**0.748**	**0.787**	**0.818**	**0.897**
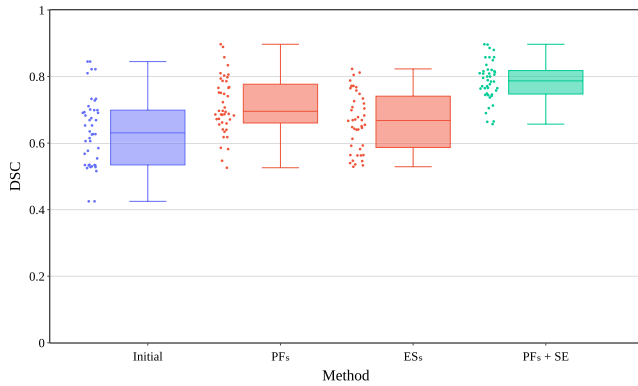
FIGURE 7. The 3D-3D rigid registration results using the PF and ES algorithms for patient and volunteer dataset for 44 image pairs. The figure shows the DSC before registration (initial) and after registration using the same (s) transform approach for the PF and ES algorithms. The DSC after rigid and non-rigid registration for PF with the same transform approach and Simple Elastix (SE) registration is shown as the last plot.

TABLE 6. The average computational time taken for 3D-3D rigid registration of images on AMD EPYC 7532 processor.

Dataset	Method	Time (Minutes)
Patient	PF_u	496
	ES_u	809
	PF_s	16
	ES_s	27
Patient + Volunteer	PF_s	15
	ES_s	26

future directions. In addition, rigid registration approaches proposed for 3DE images are also discussed. One application of the MC algorithm is the multimodal affine registration using the adaptive MC approach [16] proposed for 2D non-US medical images, where 150 test cases were obtained by applying 30 randomly generated affine transforms to 5 original aligned image sets. The adaptive sampling scheme was used, where the initial sampling density function was refined over iterations to generate more relevant solution candidates and reduce computational performance with multi resolution (scales: 1/4, 1/2, 1) approach to register images. Since the ground truth transforms were known for all 150 test cases, root mean square error (RMSE) was used to evaluate the accuracy of the method by 30 trials. Each trial used 100 iterations where the best transform solution was selected from 100 different candidates introduced in each iteration using Pearson type-VII error between phase moments of the images as an objective function. The accuracy of the method was reported as the minimum, mean, and maximum RMSE values, reporting low values compared to other baseline methods. The efficiency of the algorithm was evaluated by distorting images with 30 affine transforms over 12 ranges. The method performed well with a small number of solution candidates when there was a large misregistration and little or no region overlap between images. Compared to this approach, the sequential MC approach proposed in our study is quite challenging and novel because of the noise level and artifacts present in US images, the higher image dimension, and the evaluation of the accuracy when ground truth transforms are not known. The other advantage of the sequential MC approach is that it considers the weighted mean of all states instead of selecting one solution candidate to account for the nonlinearity of 3D image domain, even though the adaptive sampling approach helps to generate more relevant candidates over iterations.

In another MC based approach [17], affine registration was performed on 2D-2D and 3D-3D non-US images, ignoring the shear transform. A 256×256 T1 MRI brain image was registered with 16 different T2 MRI images obtained by applying different known random affine transforms to the original T2 image that was perfectly aligned with the T1 image. 200 particles were used to represent the state, and registration was performed over 100 iterations with mutual information (MI) as the likelihood function. The mean value of states was considered as the final transform at the end of each iteration similar to our approach. The accuracy was tested over 100 trials using true relative mean error

Figures 8, 9, and 10 for axial, coronal, and sagittal views. The student paired t test was performed to evaluate the significance of the PF and ES algorithms using both patient and volunteer dataset, and it was found that PF results are significant compared to ES with a p value of 0.00002 at the 0.05 significance level. The correlation between DSC and NCC for approaches listed in Table 4 is shown in Figure 11 and it is found that the correlation value between DSC and NCC is 0.73. The average computational time of the PF and ES algorithms to perform 3D-3D rigid registration of images on AMD EPYC 7532 processor is reported in Table 6.
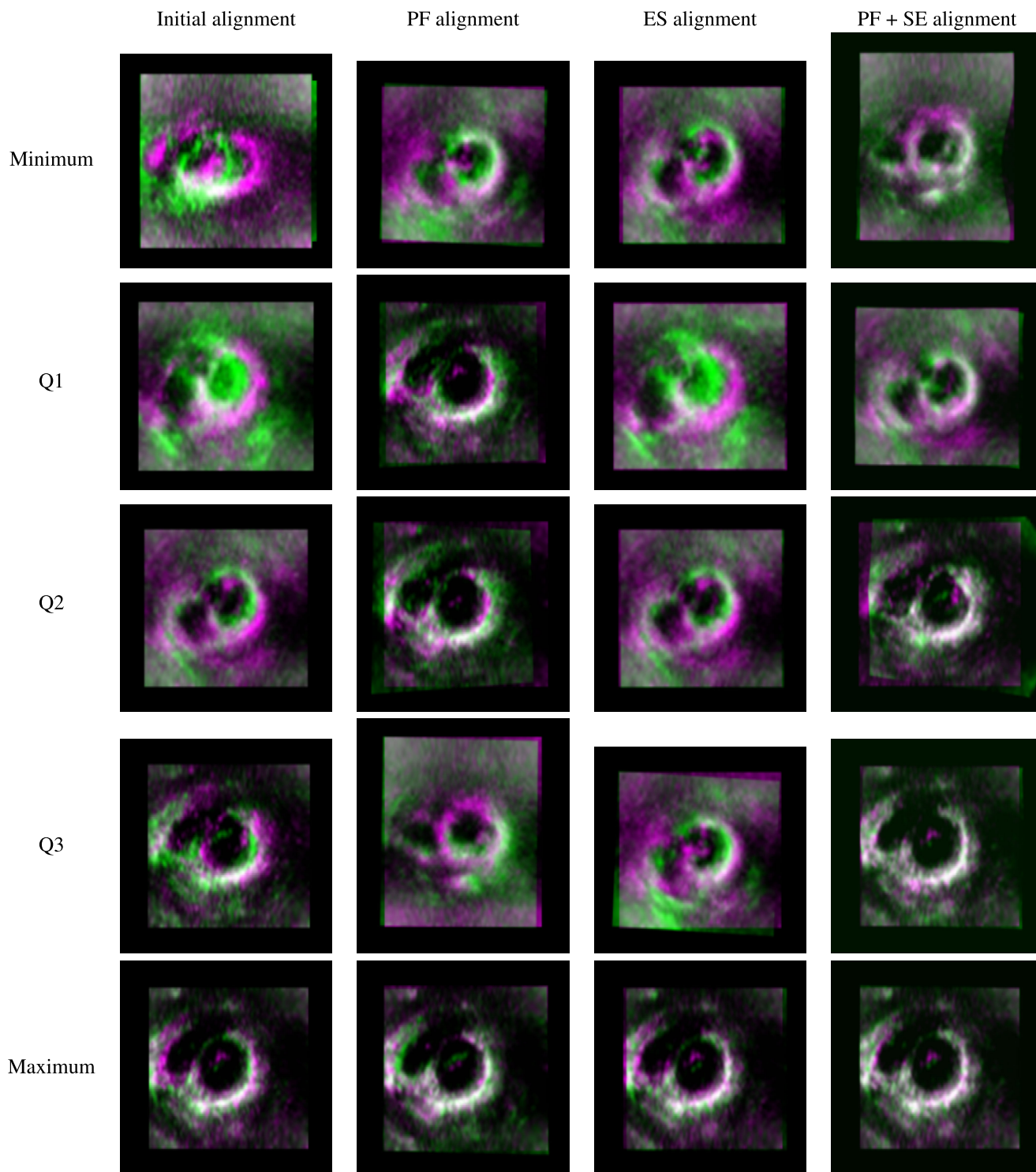
IV. DISCUSSION

This section compares the sequential MC algorithm proposed in this study with existing MC based approaches for medical image registration, the limitations of its application, and

FIGURE 8. Rigid (PF, ES) and non-rigid (SE) registration results of the first frame of image pairs for minimum (0%), Q1 (25%), Q2 (50%), Q3 (75%) and maximum (100%) DSC values of axial view, respectively. The source and target images are shown in green and purple colors.

(TRME). They performed multimodal 3D registration as three experiments that considered 10 volumes for each image pair and evaluated the accuracy using target registration error (TRE) with the minimum, mean, and maximum values

claiming that values were less than the maximum axis resolution. The first two experiments considered registering the CT and PET volumes of a patient with different types of MRI images (CT-MRI and PET-MRI), and the last
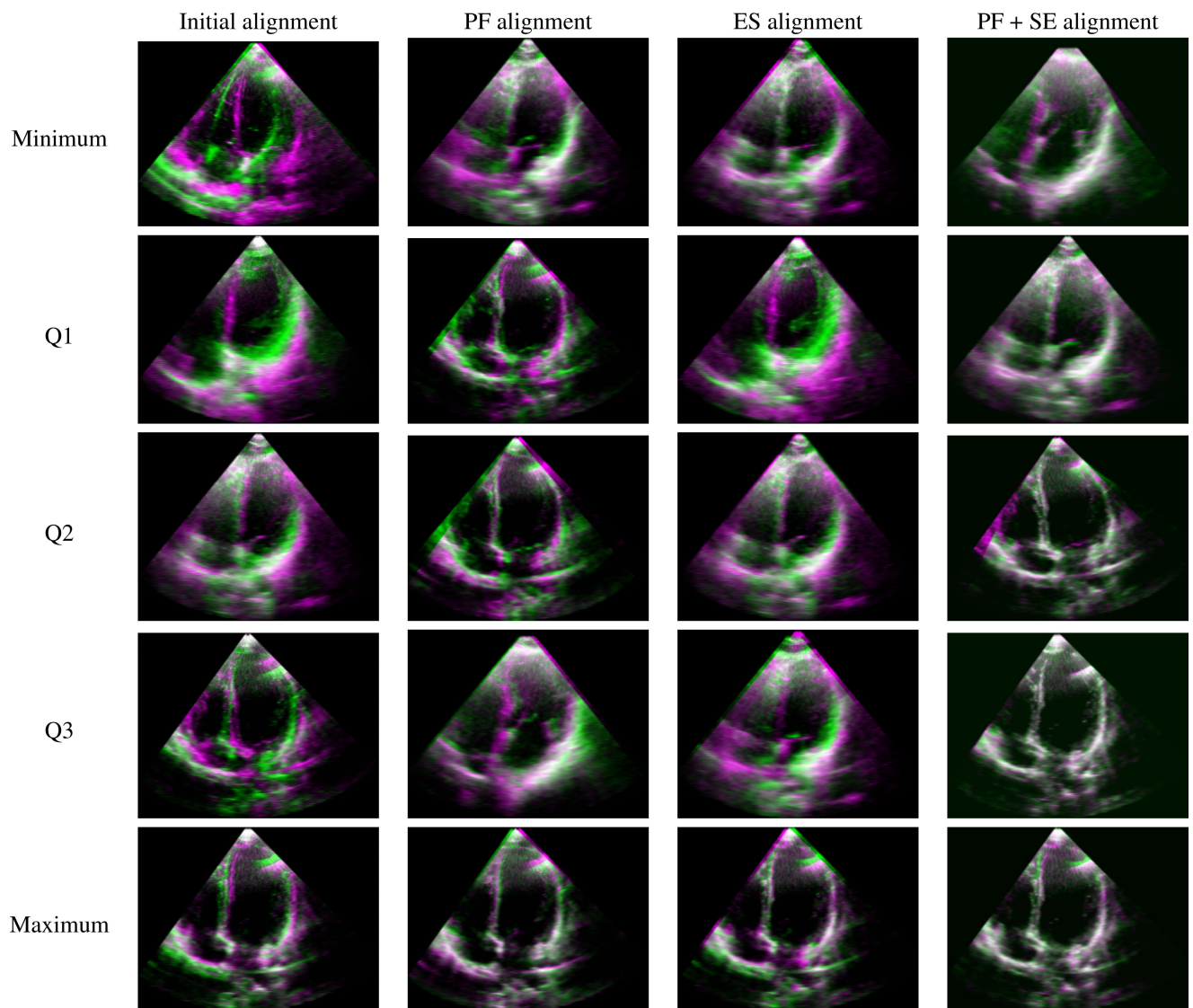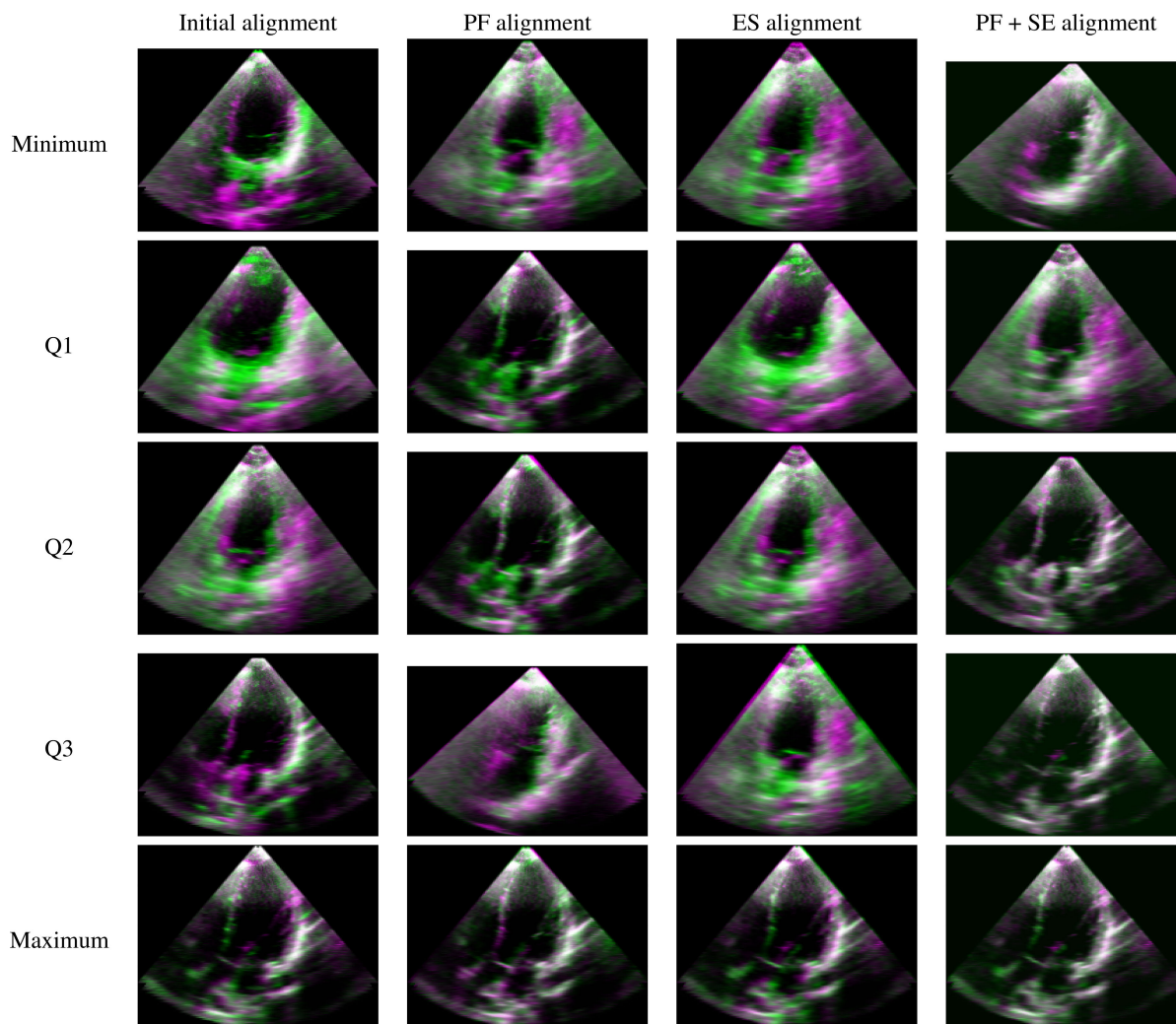
FIGURE 9. Rigid (PF, ES) and non-rigid (SE) registration results of the first frame of image pairs for min (0%), Q1 (25%), Q2 (50%), Q3 (75%) and max(100%) DSC values of coronal view, respectively. The source and target images are shown in green and purple colors.

experiment considered the CT-MRI volume registration of 7 patients. We are not able to evaluate our approach using TRE because of an unknown ground truth. The similarity metric they used was MI as it was a multimodality registration that is NCC for our approach for monomodality registration.

The particle flow filter (PFF) used in a recent study [12] for 2D and 3D rigid registration of non-medical images and 2D brain images claims to be more efficient than the PF due to fewer processing steps and a smaller number of particles. When considering the 2D-2D brain MRI image registration, the source image was generated synthetically by applying a random transform generated using 100 trials to the target image. The images were registered by adding three levels of noise (no noise, medium, and high) and then converting the intensity images to point clouds using the Matlab edge detection function. The authors claimed

that the PFF performed well compared to the PF for all three levels of noise. Since our algorithm aligns 3D-3D real echocardiographic images with their inherent noise and artifacts, we are not able to make a direct comparison to their method and they used sum of squared distance (SSD) for 2D images while we are using NCC, which is more appropriate for intensity based image registration of 3D images to consider the intensity changes in neighborhood voxels without using one to one relationships between voxels.

We implemented the PF and the ES algorithms and tested for 2D-2D registration first and then extended to 3D-3D registration considering the complexity of state space representation and algorithm parameters such as the number of particles, rotation and translation limit for the PF algorithm, and step size, scaling of rotation and translation, and optimizer step length for the ES. These parameters

FIGURE 10. Rigid (PF, ES) and non-rigid (SE) registration results of the first frame of image pairs for min (0%), Q1 (25%), Q2 (50%), Q3 (75%) and max(100%) DSC values of sagittal view, respectively. The source and target images are shown in green and purple colors.
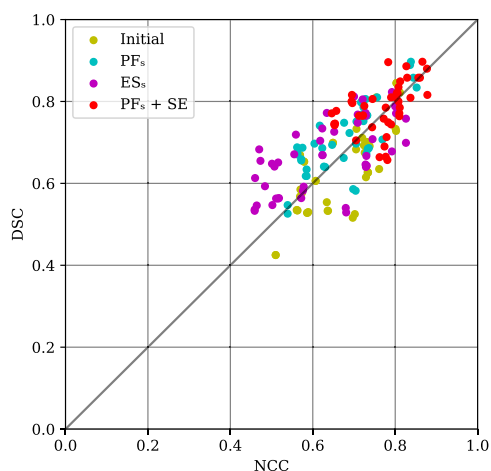
FIGURE 11. The correlation between overlapping score (DSC) and similarity metric (NCC) of PF, ES, and PF + SE methods for patient and volunteer data.

remain the same for both 2D and 3D images. The best parameters were found using the grid search approach over the entire dataset. If these algorithms need to be applied to a new data set, these parameters need to be fine tuned to get better performance. The results of the PF and ES algorithms show that the sequential MC approach is more efficient compared to the ES, considering NCC and Dice score metric values.

All the MC based algorithms, including the one proposed by us, have not been implemented for parallel architecture or non-rigid registration yet, and there is great potential for it as a future work. A recent study [23] proposed a combination of rigid and non-rigid algorithms for 3D-3D echocardiographic image registration, where landmark based rigid registration was performed using a reinforcement learning model. Compared to that approach, the SMC based rigid registration proposed in this study is a training free, pairwise registration approach that uses image intensity instead of landmarks.

V. CONCLUSION

The proposed intensity based 3D-3D rigid registration of echocardiographic images with significant overlap using a

sequential Monte Carlo algorithm performs well compared to the exhaustive search algorithm in terms of accuracy. Moreover, registering images using the same transform gives the overall best performance in terms of computational time against the unique transform approach while offering very similar alignment accuracy measured in terms of the Dice score for the left ventricle. The parallel version of the algorithm is being implemented, and it will be used to align 3D images in future work.

ACKNOWLEDGMENT

REFERENCES

[1] Cardiovascular Diseases (CVDs). Accessed: Sep. 13, 2023. [Online]. Available: https://www.who.int/news-room/fact-sheets/detail/cardiovascular-diseases-(cvds)

[2] Heart Disease in Canada. Accessed: Sep. 13, 2023. [Online]. Available: https://www.canada.ca/en/public-health/services/publications/diseases-conditions/heart-disease-canada.html

[3] A. Ghorbani, D. Ouyang, A. Abid, B. He, J. H. Chen, R. A. Harrington, D. H. Liang, E. A. Ashley, and J. Y. Zou, "Deep learning interpretation of echocardiograms," NPJ Digit. Med., vol. 3, no. 1, p. 10, Jan. 2020. [Online]. Available: https://www.nature.com/articles/s41746-019-0216-8

[4] S. Liu, Y. Wang, X. Yang, B. Lei, L. Liu, S. X. Li, D. Ni, and T. Wang, "Deep learning in medical ultrasound analysis: A review," Engineering, vol. 5, no. 2, pp. 261–275, Apr. 2019. [Online]. Available: https://linkinghub.elsevier.com/retrieve/pii/S2095809918301887

[5] C. Che, T. S. Mathai, and J. Galeotti, "Ultrasound registration: A review," Methods, vol. 115, pp. 128–143, Feb. 2017. [Online]. Available: https://linkinghub.elsevier.com/retrieve/pii/S1046202316304789

[6] K. Cleary and T. M. Peters, "Image-guided interventions: Technology review and clinical applications," Annu. Rev. Biomed. Eng., vol. 12, no. 1, pp. 119–142, Jul. 2010. [Online]. Available: http://www.annualreviews.org/doi/10.1146/annurev-bioeng-070909-105249

[7] Y. Fu, Y. Lei, T. Wang, W. J. Curran, T. Liu, and X. Yang, "Deep learning in medical image registration: A review," Phys. Med. Biol., vol. 65, no. 20, 2020, Art. no. 20TR01. [Online]. Available: https://iopscience.iop.org/article/10.1088/1361-6560/ab843e

[8] C. Fookes and M. Bennamoun, "Rigid medical image registration and its association with mutual information," Int. J. Pattern Recognit. Artif. Intell., vol. 17, no. 7, pp. 1167–1206, Nov. 2003. [Online]. Available: https://www.worldscientific.com/doi/abs/10.1142/S0218001403002800

[9] R. M. Lang et al., "EAE/ASE recommendations for image acquisition and display using three-dimensional echocardiography," J. Amer. Soc. Echocardiogr., vol. 25, no. 1, pp. 3–46, Jan. 2012. [Online]. Available: https://academic.oup.com/ehjcimaging/article-lookup/doi/10.1093/ehjci/jer316

[10] R. Shams, P. Sadeghi, R. A. Kennedy, and R. I. Hartley, "A survey of medical image registration on multicore and the GPU," IEEE Signal Process. Mag., vol. 27, no. 2, pp. 50–60, Mar. 2010. [Online]. Available: http://ieeexplore.ieee.org/document/5438962/

[11] D. Grzech, M. F. Azampour, B. Glocker, J. Schnabel, N. Navab, B. Kainz, and L. L. Folgoc, "A variational Bayesian method for similarity learning in non-rigid image registration," in Proc. IEEE/CVF Conf. Comput. Vis. Pattern Recognit. (CVPR), New Orleans, LA, USA, Jun. 2022, pp. 119–128. [Online]. Available: https://ieeexplore.ieee.org/document/9879941/

[12] S. R. Porter, "Point set registration via stochastic particle flow filter," Proc. SPIE, vol. 30, no. 6, pp. 063007-1–063007-21, Nov. 2021. [Online]. Available: https://www.spiedigitallibrary.org/journals/journal-of-electronic-imaging/volume-30/issue-06/063007/Point-set-registration-via-stochastic-particle-flow-filter/10.1117/1.JEI.30.6.063007.full

[13] D. Berg, H. H. Bauser, and K. Roth, "Covariance resampling for particle filter—State and parameter estimation for soil hydrology," Hydrol. Earth Syst. Sci., vol. 23, no. 2, pp. 1163–1178, Feb. 2019. [Online]. Available: https://hess.copernicus.org/articles/23/1163/2019/

[14] M. S. Arulampalam, S. Maskell, N. Gordon, and T. Clapp, "A tutorial on particle filters for online nonlinear/non-Gaussian Bayesian tracking," IEEE Trans. Signal Process., vol. 50, no. 2, pp. 174–188, Feb. 2002.

[15] J. Elfring, E. Torta, and R. van de Molengraft, "Particle filters: A hands-on tutorial," Sensors, vol. 21, no. 2, p. 438, Jan. 2021. [Online]. Available: https://www.mdpi.com/1424-8220/21/2/438

[16] A. Wong, "An adaptive Monte Carlo approach to phase-based multimodal image registration," IEEE Trans. Inf. Technol. Biomed., vol. 14, no. 1, pp. 173–179, Jan. 2010. [Online]. Available: http://ieeexplore.ieee.org/document/5308332/

[17] E. R. Arce-Santana, D. U. Campos-Delgado, and A. Alba, "Affine image registration guided by particle filter," IET Image Process., vol. 6, no. 5, p. 455, 2012. [Online]. Available: https://digital-library.theiet.org/content/journals/10.1049/iet-ipr.2011.0083

[18] A. R. Mejia-Rodriguez, E. R. Arce-Santana, E. Scalco, D. Tresoldi, M. O. Mendez, A. M. Bianchi, G. M. Cattaneo, and G. Rizzo, "Elastic registration based on particle filter in radiotherapy images with brain deformations," in Proc. Annu. Int. Conf. IEEE Eng. Med. Biol. Soc., Boston, MA, USA, Aug. 2011, pp. 8049–8052. [Online]. Available: http://ieeexplore.ieee.org/document/6091985/

[19] M. Abdel-Basset, A. E. Fakhry, I. El-henawy, T. Qiu, and A. K. Sangaiah, "Feature and intensity based medical image registration using particle swarm optimization," J. Med. Syst., vol. 41, no. 12, p. 197, Dec. 2017.

[20] D. Grzech, M. F. Azampour, H. Qiu, B. Glocker, B. Kainz, and L. Le Folgoc, "Uncertainty quantification in non-rigid image registration via stochastic gradient Markov chain Monte Carlo," Mach. Learn. Biomed. Imag., vol. 1, pp. 1–25, Oct. 2021.

[21] L. Martino, V. Elvira, and F. Louzada, "Effective sample size for importance sampling based on discrepancy measures," Signal Process., vol. 131, pp. 386–401, Feb. 2017. [Online]. Available: https://www.sciencedirect.com/science/article/pii/S0165168416302110

[22] G. Balakrishnan, A. Zhao, M. R. Sabuncu, J. Guttag, and A. V. Dalca, "VoxelMorph: A learning framework for deformable medical image registration," IEEE Trans. Med. Imag., vol. 38, no. 8, pp. 1788–1800, Aug. 2019. [Online]. Available: https://ieeexplore.ieee.org/document/8633930/

[23] S. Shanmuganathan, M. Noga, P. Boulanger, B. Foster, H. Becher, and K. Punithakumar, "Two-step rigid and non-rigid image registration for the alignment of three-dimensional echocardiography sequences from multiple views," IEEE Access, vol. 12, pp. 53485–53496, 2024. [Online]. Available: https://ieeexplore.ieee.org/document/10497605/

[24] M. P. Henry, J. I. Cotella, J. A. Slivnick, M. Yamat, K. Hipke, R. Johnson, V. Mor-Avi, and R. M. Lang, "Three-dimensional echocardiographic deconstruction: Feasibility of clinical evaluation from two-dimensional views derived from a three-dimensional data set," J. Amer. Soc. Echocardiography, vol. 35, no. 10, pp. 1009–1017, Oct. 2022. [Online]. Available: https://www.ncbi.nlm.nih.gov/pmc/articles/PMC10231028/

[25] S. Robinson et al., "A practical guideline for performing a comprehensive transthoracic echocardiogram in adults: The British Society of Echocardiography minimum dataset," Echo Res. Pract., vol. 7, no. 4, pp. G59–G93, Dec. 2020. [Online]. Available: https://echo.biomedcentral.com/articles/10.1530/ERP-20-0026

[26] E. Ostenfeld, K. Shahgaldi, R. Winter, R. Willenheimer, and J. Holm, "Comparison of different views with three-dimensional echocardiography: Apical views offer superior visualization compared with parasternal and subcostal views," Clin. Physiol. Funct. Imag., vol. 28, no. 6, pp. 409–416, Nov. 2008. [Online]. Available: https://onlinelibrary.wiley.com/doi/10.1111/j.1475-097X.2008.00823.x

[27] J. Hung, R. Lang, F. Flachskampf, S. K. Shernan, M. L. McCulloch, D. B. Adams, J. Thomas, M. Vannan, and T. Ryan, "3D echocardiography: A review of the current status and future directions," J. Amer. Soc. Echocardiography, vol. 20, no. 3, pp. 213–233, Mar. 2007. [Online]. Available: https://linkinghub.elsevier.com/retrieve/pii/S0894731707000181

[28] T. Rohlfing, "Image similarity and tissue overlaps as surrogates for image registration accuracy: Widely used but unreliable," IEEE Trans. Med. Imag., vol. 31, no. 2, pp. 153–163, Feb. 2012. [Online]. Available: http://ieeexplore.ieee.org/document/5977031/

[29] K. Punithakumar, M. Noga, P. Boulanger, and H. Becher, "Integration of robotic technology for combining multiple views in three-dimensional echocardiography," in Proc. 28th Int. Conf. Autom. Comput. (ICAC), Birmingham, U.K., Aug. 2023, pp. 1–6. [Online]. Available: https://ieeexplore.ieee.org/document/10275274/

[30] K. Marstal, F. Berendsen, M. Staring, and S. Klein, "SimpleElastix: A user-friendly, multi-lingual library for medical image registration," in *Proc. IEEE Conf. Comput. Vis. Pattern Recognit. Workshops (CVPRW)*, Las Vegas, NV, USA, Jun. 2016, pp. 574–582. [Online]. Available: http://ieeexplore.ieee.org/document/7789568/

[31] H. J. Johnson and M. M. McCormick, *The ITK Software Guide Book 2: Design and Functionality*, 4th ed. Insight Software Consortium, Aug. 2021. [Online]. Available: https://insightsoftwareconsortium.org/

THANUJA URUTHTHIRAKODEESWARAN (Member, IEEE) received the B.Sc.Eng. degree (Hons.) in computer science and engineering from the University of Moratuwa, Sri Lanka, in 2015. She is currently pursuing the Ph.D. degree with the Department of Radiology and Diagnostic Imaging, University of Alberta, Canada, under the supervision of Dr. Kumaradevan Punithakumar and Dr. Lawrence Le. Her professional journey commenced as a Trainee Software Engineer with Virtusa (Pvt.) Ltd., from November 2013 to April 2014. Following that, she was a Software Engineer with WSO2 (Pvt.) Ltd., where she made contributions to open-source projects, from May 2015 to Feb 2017, before joining Proavos (Pvt.) Ltd. Since June 2017, she has been a Lecturer with the Department of Computer Engineering, University of Jaffna, Sri Lanka. Her research interests include medical image analysis, software engineering, and artificial intelligence.

MICHELLE NOGA is currently a Radiologist trained with the University of Alberta and British Columbia's Children's and Women's Hospital. She is also a Professor with the Department of Radiology and Diagnostic Imaging, University of Alberta, and a Radiologist with medical imaging consultants. She established the first cardiac MRI Program at Alberta and has successfully established the first center for the virtual 3D display of cardiac imaging in a clinical setting, a product of a 1 000 000 Grant from Servier Canada. She has published over 80 publications and conference proceedings and holds three patents. Her research interests include pediatric cardiac MRI and CT, post-processing of cross-sectional cardiac imaging, 3D visualization, rapid prototyping, pediatric airway, and finite element analysis.

LAWRENCE H. LE received the Ph.D. degree in Earth physics and the M.B.A. degree in finance and technology commercialization from the University of Alberta, Edmonton, AB, Canada, in 1991 and 1999, respectively. He held a Natural Sciences and Engineering Research Council of Canada (NSERC) Postdoctoral Fellowship with Schlumberger-Doll Research, Ridgefield, CT, USA. He started his medical physics training with the Department of Radiology and Diagnostic Imaging (DRDI), University of Alberta, in 1994. He joined DRDI, University of Alberta, as a Clinical Academic Staff, and Capital Health, Edmonton, as a Clinical Medical Physicist, in 2000. He is currently a Clinical Professor leading the Graduate Program at DRDI, University of Alberta, and a Senior Medical Physicist with Alberta Health Services, Edmonton. He is also a Senior Visiting Scholar with the Center for Biomedical Engineering, Fudan University, Shanghai, China. His research interests include ultrasound imaging, signal and image processing, wave propagation modeling and inversion, and machine learning. He is a member of American Association of Physicists in Medicine (AAPM) and Canadian Organization of Medical Physicists (COMP).

PIERRE BOULANGER (Member, IEEE) was a Senior Research Officer with the National Research Council of Canada, for 18 years. He has a double appointment as a Professor with the Department of Computing Science and the Department of Radiology and Diagnostic Imaging, University of Alberta. He is currently the Director of the Advanced Human–Computer Interface Laboratory (AHCI) and the Scientific Director of the Servier Virtual Cardiac Centre. He cumulates more than 40 years of experience in 3D computer vision, rapid product development, and the applications of virtual reality systems to medicine and industrial manufacturing. His research interests include 3D computer vision, rapid product development, and virtualized reality systems.

HARALD BECHER is currently an Emeritus Professor of Medicine. He joined the University of Alberta and the Mazankowski Alberta Heart Institute, in 2010. He held the position of the Heart and Stroke Foundation of Alberta, NWT, and the Nunavut Chair of Cardiovascular Research for ten years. He is the author of more than 100 scientific articles and has written 24 book chapters. His research interests include medical image analysis, stress echocardiography, and contrast echocardiography. He is a section editor of the *journal Echocardiography*.

KUMARADEVAN PUNITHAKUMAR (Senior Member, IEEE) received the B.Sc.Eng. degree (Hons.) in electronic and telecommunication engineering from the University of Moratuwa and the M.A.Sc. and Ph.D. degrees in electrical and computer engineering from McMaster University. From 2001 to 2002, he was an Instructor with the Department of Electronic and Telecommunication Engineering, University of Moratuwa. In 2008, he was a Postdoctoral Research Fellow with the Department of Electrical and Computer Engineering, McMaster University. From 2008 to 2012, he was an Imaging Research Scientist with GE Healthcare, Canada. He is currently an Associate Professor and the AHS Chair of diagnostic imaging with the Department of Radiology and Diagnostic Imaging, University of Alberta, and the Operational and Computational Director of the Servier Virtual Cardiac Centre, Mazankowski Alberta Heart Institute. His research interests include medical image analysis and visualization, information fusion, object tracking, and nonlinear filtering. He was a recipient of the Industrial Research and Development Fellowship from the National Sciences and Engineering Research Council of Canada, in 2008.

• • •